Molecular Biology of the Cell
Vol. 15, 4597–4608, October 2004

Defective Epidermal Barrier in Neonatal Mice Lacking the C-Terminal Region of Connexin43[D][V]

Karen Maass,* Alexander Ghanem,† Jung-Sun Kim,‡ Manuela Saathoff,§ Stephanie Urschel,* Gregor Kirfel,§ Ruth Grümmer,‖ Markus Kretz,* Thorsten Lewalter,† Klaus Tiemann,† Elke Winterhager,‖ Volker Herzog,§ and Klaus Willecke*¶

*Institut für Genetik, Universität Bonn, D-53117 Bonn, Germany; †Medizinische Klinik und Poliklinik II, Kardiologie und Pneumologie, Universität Bonn, D-53105 Bonn, Germany; ‡University of Ulsan, College of Medicine, Seoul, Republic of Korea; §Institut für Zellbiologie, Universität Bonn, D-53121 Bonn, Germany; and ‖Medizinische Fakultät der Universität Duisburg-Essen, D-45122 Essen, Germany

Submitted April 20, 2004; Revised July 9, 2004; Accepted July 13, 2004
Monitoring Editor: Daniel Goodenough

More than 97% of mice in which the C-terminal region of connexin43 (Cx43) was removed (designated as Cx43K258stop) die shortly after birth due to a defect of the epidermal barrier. The abnormal expression of Cx43K258stop protein in the uppermost layers of the epidermis seems to perturb terminal differentiation of keratinocytes. In contrast to Cx43-deficient mice, neonatal Cx43K258stop hearts show no lethal obstruction of the right ventricular outflow tract, but signs of dilatation. Electrocardiographies of neonatal hearts reveal repolarization abnormalities in 20% of homozygous Cx43K258stop animals. The very rare adult Cx43K258stop mice show a compensation of the epidermal barrier defect but persisting impairment of cardiac function in echocardiography. Female Cx43K258stop mice are infertile due to impaired folliculogenesis. Our results indicate that the C-terminally truncated Cx43K258stop mice lack essential functions of Cx43, although the truncated Cx43 protein can form open gap junctional channels.

INTRODUCTION

Gap junctions are intercellular protein conduits allowing direct metabolic and electrical coupling of contacting cells by diffusional exchange of ions, metabolites, and second messengers up to a molecular mass of 1 kDa (Evans and Martin, 2002; Willecke *et al.*, 2002). They are formed between adjacent cells, each contributing a hemichannel consisting of six protein subunits, termed connexins. To date, 20 mouse and 21 human connexins have been identified (Söhl and Willecke, 2003), which seem to share the topology of transmembrane proteins transversing the lipid bilayer four times, with amino and carboxy termini oriented toward the cytoplasm. Connexin isoforms are cell type specifically expressed and assemble into channels that differ from each other by their unitary conductance (Suchyna *et al.*, 1999), permeability (Niessen at al., 2000; Qu and Dahl, 2002), and regulation (Lampe and Lau, 2000; Harris, 2001). The highest sequence diversity between connexin isoforms resides in the cytoplasmic loop and carboxy-terminal region. Connexin43 (Cx43), which is the most abundant mammalian connexin and one of the best-studied isoforms, is regulated by different mechanisms involving the C-terminal region. Several phosphorylation sites for different kinases are present in this domain consisting of 156 amino acids (Musil *et al.*, 1990). Phosphorylation of Cx43 has been implicated in the regulation of gap junctional intercellular communication (GJIC) (Kim *et al.*, 1999; Lampe *et al.*, 2000). Regulation of GJIC upon acidification can be explained by an intramolecular ball-and-chain closure mechanism (Liu *et al.*, 1993, Delmar *et al.*, 2004), whereby amino acid residues of the cytoplasmic loop act as receptor to which the C terminus can bind (Duffy *et al.*, 2002). Impaired channel closure due to deletion of the last 125 amino acids of the C terminus could be rescued by coexpression of the C-terminal fragment in *Xenopus* oocytes (Morley *et al.*, 1996). This gating mechanism also has been observed in the regulation of Cx43 gap junctional channels by insulin/insulin-like growth factor (Homma *et al.*, 1998), platelet-derived growth factor (Moorby and Gherardi, 1999), v-src (Zhou *et al.*, 1999), and transjunctional voltage (Moreno *et al.*, 2002). Apart from this intramolecular protein–protein interaction, the C terminus of Cx43 can directly bind to other proteins. Binding sites for Zonula occludens protein ZO-1 (Giepmans and Moolenaar, 1998), c-scr, as well as α- and β-tubulin (Giepmans *et al.*, 2001a,b) have been identified. Point mutations in human Cx43 have been connected to oculodentodigital dysplasia (Paznekas *et al.*, 2003) and hypoplastic left heart syndrome (Dasgupta *et al.*, 2001). Transgenic mice deficient for Cx43 do not show the symptoms these diseases, because these animals die shortly after birth

Article published online ahead of print. Mol. Biol. Cell 10.1091/mbc.E04–04–0324. Article and publication date are available at www.molbiolcell.org/cgi/doi/10.1091/mbc.E04–04–0324.

[D][V] The online version of this article contains supplemental material accessible through http://www.molbiolcell.org.

¶ Corresponding author. E-mail address: genetik@uni-bonn.de.

Abbreviations used: Cx, connexin; HE, hematoxytin & eosin, HO, homozygous; HT, heterozygous; GJIC, gap junction intercellular communication; HPRT, hypoxanthine-guanine phosphoribosyl transferase; PGK, phosphoglycerate kinase; QT_c, heart frequency corrected QT-interval, s., stratum, SEM, scanning electron microscopy, TEM, transmission electron microscopy; WT, wild-type.

due to obstructions of the right ventricular outflow tract of the heart (Reaume *et al.*, 1995). To further correlate the diverse functions of the Cx43 protein to its C-terminal region, we decided to delete the C-terminal 125 amino acid residues in transgenic mice (designated as Cx43K258stop mice). Surprisingly, we found that >97% of these homozygous mutant mice die shortly after birth, due to a defective epidermal permeability barrier.

MATERIALS AND METHODS

Generation of Mice

Cx43K258stop mice were generated by gene double replacement in *hprt*-deficient HM1 cells (Stacey *et al.*, 1994) as described previously by Plum *et al.*, 2000 (Figure 1). Homologously recombined embryonic stem cell clones were injected into C57BL/6 blastocysts as described by Hogan *et al.* (1994) to generate chimeras that were subsequently tested for germ line transmission of the *cx43K258stop* allele by mating to C57BL/6 mice. All analyses were carried out on mixed 129/Ola/C57BL/6 genetic background by using littermates as controls. Mice were kept under standard housing conditions with a fixed 12/12-h light/dark cycle. C57BL/6 mice were obtained from Charles River (Sulzfeld, Germany). All experiments were carried out according to German law for protection of animals and with prior permission by local government authorities.

Sample Collection

For histopathological investigations, tissues of neonates and ovaries of adult animals at estrous were taken, fixed for 2 h (epidermis) or overnight with 2% paraformaldehyde (PFA) in phosphate-buffered saline (PBS), dehydrated, and embedded in paraffin. Sections were stained with hematoxylin & eosin (HE); coverslips were mounted with Entellan (Merck, Darmstadt, Germany) and photographed using an Axiophot microscope (Carl Zeiss, Oberkochem, Germany) equipped with a charge-coupled device (CCD) camera (Carl Zeiss) and AxioVision software (Carl Zeiss). Samples for immunofluorescence analysis were frozen on dry ice and subsequently processed to 5- to 10-μm cryosections. Samples for immunoblot analysis were snap-frozen in liquid nitrogen; the epidermis was separated before from dermis by 30-s incubation in PBS at 60°C. Tissues were grounded, lyophilized overnight, and subsequently dissolved in adjusted volumes of Laemmli buffer (Laemmli, 1970), including 4% Complete proteinase inhibitor (Roche Diagnostics, Basel, Switzerland).

Toluidine Blue Penetration Assay

Staining of neonates was performed as described by Hardman *et al.* (1998). Animals were photographed directly with a digital camera (Power Shot; Canon, Tokyo, Japan) mounted onto a binocular microscope (MS5; Leica, Solms, Germany).

Transmission Electron Microscopy (TEM)

Pieces (1 × 1 mm) of epidermis were fixed in 2% glutaraldehyde and 4% PFA in 0.1 M sodium cacodylate buffer (pH 7.3) for 60 min at room temperature (RT); rinsed in sodium cacodylate buffer; and postfixated with 2% unbuffered osmium tetroxide for 60 min at 4°C, followed by staining en bloc with 4% unbuffered uranyl acetate for 90 min at RT. Samples were dehydrated through a graded series of ethanol, cleared in propylene oxide, and embedded in Epoxy embedding medium (Fluka, Buchs, Switzerland). Thin sections were stained with 4% unbuffered uranyl acetate for 20 min and subsequently with 2.5% unbuffered lead citrate for 10 min and examined at 80 kV with a CM 120 (Philips Electron Optics, Eindhoven, The Netherlands) equipped with a LaB_6 filament.

Scanning Electron Microscopy (SEM)

Tissue samples were fixed with 2% glutaraldehyde in 0.1 M sodium cacodylate buffer (pH 7.3) for 60 min at RT, rinsed in sodium cacodylate buffer, and dehydrated through a graded series of ethanol. Samples were critical point dried from CO_2 in 10 cycles according to Svitkina *et al.* (1984) by using a Balzers CPD 030 (BAL-TEC, Schalksmühlen, Germany). Dried samples were mounted on aluminum sample holders and sputter coated with 2-nm platinum/palladium in an HR 208 coating device (Cressington, Watford, United Kingdom). SEM was performed at an acceleration voltage of 3 kV by using an XL 30 SFEG (Philips) equipped with a through lens secondary electron detector.

Immunofluorescence Analysis

Cryosections were incubated with rabbit polyclonal antibodies directed to keratin1, keratin5, loricrin, filaggrin (Babco, CRP, Cumberland, VA), ZO-1 (Zymed Laboratories, South San Francisco, CA), the cytoplasmic loop of Cx43 (Yeager and Gilula, 1992), Cx31 (BioTrend, Cologne, Germany), Cx30 (Zymed Laboratories), or mouse monoclonal antibodies to Cx26 (Zymed Laboratories). Analyses were carried out with MOM kit (Vector Laboratories, Burlingame, CA) according to manufacturer's instructions, by using Alexa 594- or Alexa 488-conjugated, species-specific secondary antibodies (MoBiTec, Goettingen, Germany). Nuclei were stained by incubating sections in PBS including 0.5 μg/ml bisbenzimide (Hoechst 33258 stain; Sigma Chemie, Deisenhofen, Germany) for 15 min before mounting on coverslips with Permafluor

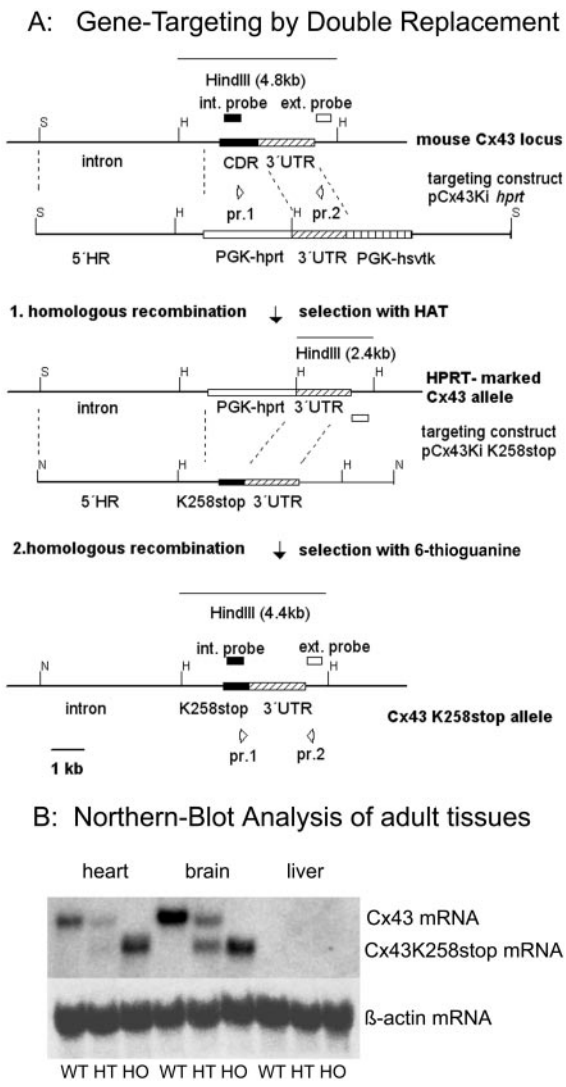

Figure 1. Gene targeting and transcription analysis of the cx43K258stop allele. In a first homologous recombination in *hprt*-deficient embryonic stem cells, the *cx43* coding region was replaced by a PGK-*hprt*-cassette (Plum *et al.*, 2000). In the second homologous recombination, the PGK-*hprt*-cassette was replaced by the truncated *cx43* coding region. Recombined clones were enriched by 6-thioguanine selection, validated by PCR analysis and Southern blot by using a 3′ external and a *cx43* internal probe. S, *Sac*I; H, *Hind*III; N, *Not*I; int, internal; ext., external; CDR, coding region; UTR, untranslated region; HR, homologous region; PGK-*hprt*, phosphoglycerate kinase promoter-hypoxanthine-guanine phosphoribosyl transferase-minigene; PGK-*hsvtk*, phosphoglycerate kinase promoter-hepes simplex virus thymidine kinase cassette; Ki, knockin. (B) Total RNA blot of heart, brain and liver of WT, HT, and HO adult animals was probed with a radiolabeled DNA fragment corresponding to *cx43* 5′-UTR. The 2.6-kb *cx43K258stop* transcript was detected proportional to gene dosis. No 3.0-kb *cx43* wild-type transcript was detected in homozygous mutant animals. Equal amounts of loaded total RNA were verified by reprobing with a *β-actin* probe.

(Immunotec, Marseille, France). Samples were photographed at RT by using an Axiophot microscope (Carl Zeiss) equipped with a CCD camera (Carl Zeiss) and AxioVision software (Carl Zeiss). Controls in the absence of primary antibodies were routinely performed and yielded no signals. Figures were composed with the help of Adobe Photoshop software (version 6.0; image procession restricted to changes in brightness and contrast of whole images).

Immunoblot Analysis

Equal protein amounts were determined using the bicinchoninic acid protein determination kit (Sigma Chemie) according to the manufacturer's instructions and separated by SDS-PAGE (Laemmli, 1970) at 25 mA per gel and electroblotted for 2 h at 100 V at 4°C onto nitrocellulose membranes (Hybond, 0.45 μm; Amersham Biosciences UK, Little Chalfont, Buckinghamshire, United Kingdom). Blots were incubated with antibodies overnight at 4°C and immunoreactive proteins were visualized by species-specific horseradish peroxidase-conjugated secondary antibodies (Dianova, Hamburg, Germany) and subsequent enhanced chemiluminescence (Amersham Biosciences UK) as recommended by the manufacturer. ECL blots were developed on x-ray film (SuperRX; Fujifilm, Tokyo, Japan). Blot could be reused after incubation with stripping buffer (RestoreTM; Pierce Chemical, Rockford, IL).

DNA Isolation and Analysis

Genomic DNA was isolated as described by Laird *et al.* (1991b). For Southern blot analysis, DNA was digested with *Hind*III, fractionated on 0.7% agarose gels and transferred onto nylon membranes (Hybond$^+$, 0.4 μm; Amersham Biosciences UK), and filters were probed with ^{32}P-radiolabeled *cx43* probes (first 772 base pairs of Cx43 coding region as internal probe, 550 base pairs outside the 3′ homologous region as external probe), washed, sealed into plastic wrap, and exposed to x-ray film (X-OMAT; Eastman Kodak, Rochester, NY). For genotyping of mice, DNA was subjected to polymerase chain reaction (PCR) analysis using the primers delCT-HO (5′-gcatcctcttcaagtctgtcttcg) and RO-delCT (5′-caaaacacccccaaggaacctag), resulting in an 851-base pair amplicon for the *cx43* allele and a 452-base pair amplicon for the *cx43K258stop* allele.

RNA Isolation and Northern Blot Analysis

Total RNA was isolated using TRIzol (Invitrogen, Renfew, United Kingdom) according to manufacturer's instructions. Fifty micrograms of RNA was fractionated on 1% agarose/0.9% formaldehyde gels, transferred to nylon membranes (Hybond N, 0.45 μm; Amersham Biosciences UK), UV-cross-linked (UV-Stratalinker 2400; Stratagene, La Jolla, CA), and hybridized to ^{32}P-labeled probes (corresponding to the 3′-untranslated region of *cx43* exon 2 or to *β-actin*). Filters were washed and exposed to x-ray film (X-OMAT; Eastman Kodak).

HeLa Cell Culture and Transfection

HeLa connexin transfectants were grown in DMEM (Life Technologies, Eggenstein, Germany), supplemented with 10% calf serum (Life Technologies), 100 μg/ml streptomycin, 100 μg/ml penicillin, and 1 μg/ml puromycin (Sigma Chemie). Cells were passaged three times per week and maintained in a 37°C incubator in a moist atmosphere with 10% CO_2. For generation of Cx43K258stop-expressing cells, the truncated version of *cx43* was generated by PCR mutagenesis and inserted into the pBEHpac18 expression vector (Horst *et al.*, 1991) under control of a SV40 promoter. HeLa wild-type cells were transfected by Lipofection (Tfx-50 reagent; Promega, Madison, WI) according to manufacturer's instructions. Puromycin-positive clones were isolated and grown under selection conditions.

Pulse-Chase Analysis and Determination of Half-Life

HeLa cells were metabolically labeled with [^{35}S]methionine for 1 h, as described by Hertlein *et al.* (1998). Medium was replaced by nonradioactive medium, supplemented with additional 15 mg/l methionine (final concentration 45 mg/l). Cells were harvested at different time points of chase. Connexin proteins were immunoprecipitated and subjected to SDS-PAGE. After fixation, gels were treated with Amplify (Amersham Biosciences, Freiburg, Germany), dried, and used for autoradiography. Densitometric signal values of scanned autoradiographies were calculated using Imagemaster 2.0 software (Amersham Biosciences). Signal intensity (intensity of optical density; IOD) was correlated to the amount of protein in the lysates. The densiometric value at 0-h chase was defined as 100%. Logarithms of the correlated IOD values were calculated and the parameters of the mathematical function lnIOD = a + bx were determined by the regression method using GraphPad Prism for the IBM-PC (GraphPad Software, San Diego, CA). The half-life was calculated on the slope of the regression function as mean of at least three pulse-chase experiments.

ECG Analysis of Neonatal Mice

Neonates (14 wild type, 29 heterozygous, and 18 homozygous) were subjected to surface ECG recordings according to Hagendorff *et al.* (1999). Surface six-lead ECG was acquired on a multichannel amplifier and converted to a digital signal for analysis (PowerLab system; ADInstruments, Milford, MA). ECG channels were amplified, filtered between 10 and 100 Hz, and sampled with a rate of 1 kHz. Serial ECG recordings were obtained from day 1 to day 6; spontaneous cycle length, heart rate, P-wave duration, PQ-interval, QRS-duration, and QT-interval were determined off-line, with QRS-duration starting at the Q-wave onset and lasting to the return of the S-wave to the isoelectric line. QT-interval was measured from the onset of the Q-wave to the end of the T-wave, which was defined as the final return of the T-wave to baseline level. The QT-interval was rate corrected (QT_c) according to Mitchell *et al.* (1998). ECG parameters were compared between the three genotypes by means of one-way analysis of variance (ANOVA) and post hoc Tukey-Kramer multiple comparisons test. Unpaired Student's *t* test was performed for differentiation within a genotype. P values < 0.05 were considered significant.

Table 1. Percentage of offspring (from heterozygous matings) surviving to adulthood

Group	Expected distribution (%)	Observed distribution (%)	No. of animals
Surviving wild type	25	19.5	81
Surviving heterozygous	50	49.9	207
Surviving Cx43K258stop	25	0.7	3
Postnatal lethal	0	29.9	124

RESULTS

Targeted Replacement of cx43 Coding DNA by cx43K258stop Mutant DNA in Transgenic Mice

Targeted replacement of *cx43* by *cx43K258stop* cDNA was achieved by the double replacement strategy (Figure 1A). Previously, the *cx43* open reading frame had been replaced by a *hypoxanthine-guanine phosphoribosyl transferase (hprt)*-minigene under control of a phosphoglycerate kinase (PGK) promoter in *hprt*-deficient HM1 embryonic stem cells (Plum *et al.*, 2000) in a first homologous recombination. To introduce the *cx43K258stop* mutation, a truncated version of *cx43* was generated by PCR mutagenesis by using isolated *cx43* DNA from a mouse 129/Sv genomic library (Stratagene) as template. Codon 258 was mutated into a stop codon, introducing an A-to-T transversion at nucleotide 772 of the coding region; the remaining downstream coding region was deleted. The targeting construct included the genomic *cx43* intron-exon 2 boundary, which had been partially deleted in the first homologous recombination. In the second homologous recombination, the PGK-*hprt* minigene was subsequently replaced, leading to the *cx43K258stop* allele (Figure 1A). One of the obtained embryonic stem cell clones, positive in PCR, Southern blot, and Northern blot analyses, was used for blastocyst injection and gave rise to viable heterozygous Cx43K258stop mice. Northern blot analysis of adult mouse tissues (Figure 1B) showed that the wild-type *cx43* transcript was decreased to 50% in heterozygous animals and absent in homozygous animals. The abundance of *cx43K258stop* transcript increased in a gene dosage-dependent manner from heterozygous to homozygous animals.

Cx43K258stop Mice Display Strongly Reduced Viability Due to a Postnatal Epidermal Barrier Defect

Monitoring the offspring of heterozygous matings revealed very high postnatal lethality of homozygous Cx43K258stop mice. Although the expected Mendelian ratio was found at birth, only 0.7% of the homozygous animals survived to adulthood (Table 1); most animals died during the first week (Figure 2). Homozygous animals could be identified by the abnormal appearance of their skin (Figure 3A), peeling off in

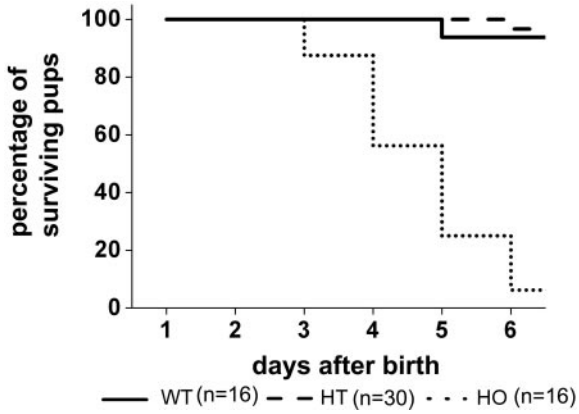

Figure 2. Homozygous Cx43K258stop mice show high postnatal lethality. Ten heterozygous matings litters (62 pups) were subjected to a close-up observation. Homozygous animals were born at the expected Mendelian ratio of 25% (16 animals) but showed high postnatal lethality with only ~2.5% (1 animal) surviving the first 5 d.

big squames, predominantly on forehead, posterior back (Figure 3B) and extremities. Constriction bands were often found around the tails of neonatal animals (Figure 3C). Because of the observed epidermal abnormalities, animals were subjected to the dye penetration assay with toluidine blue to analyze the functionality of the epidermal permeability barrier. An obvious deficiency of the epidermal permeability barrier that increased over the first days after birth was detected in homozygous Cx43K258stop mice but not in wild-type mice (Figure 3, D and E). Dye penetration was

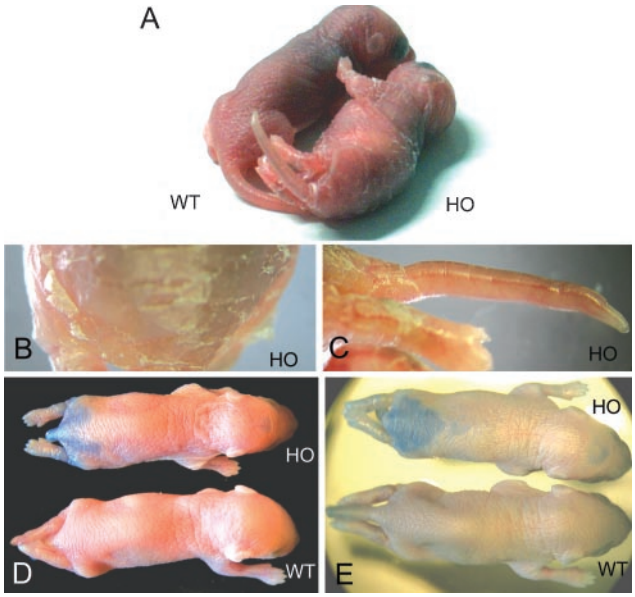

Figure 3. Homozygous Cx43K258stop pups show epidermal abnormalities and defective epidermal permeability barrier. (A–C) Comparison between littermates at postnatal day 4 revealed abnormal appearance of homozygous mutant epidermis with fissures and squames on back (A and B) and around joints (A). Constriction rings around tails were often found (C). (D and E) Penetration assays with toluidine blue revealed a defective epidermal permeability barrier of homozygous Cx43K258stop epidermis at postnatal 1 (D) and even more intensive at day 3 (E).

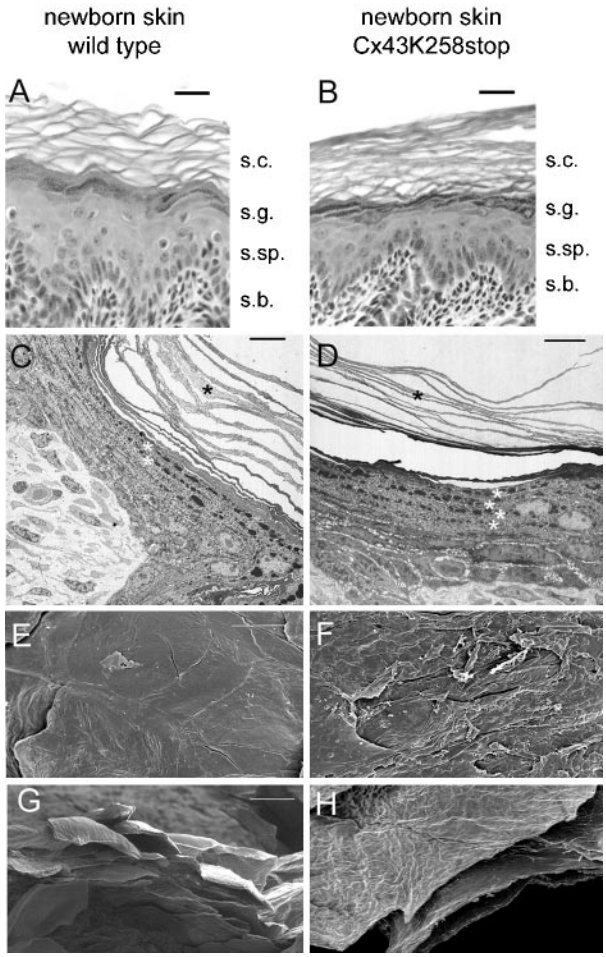

Figure 4. Comparison of wild-type and homozygous mutant epidermis by histology, transmission, and scanning electron microscopy. HE-stained paraffin sections (A and B), thin sections (C and D), and SEM of whole mount skin (E–H) revealed significant differences between morphology of s. corneum (s.c.) and s. granulosum (s.g.) of wild-type (A, C, E, and G) and homozygously mutated animals (B, D, F, and H). Characteristic of Cx43K258stop epidermis was the formation of more but thinner layers of corneocytes (C and D, black asterisks) and the premature formation of keratohyaline granules in s. spinosum (s.sp.) (C and D, white asterisks). In contrast to the even surface of wild-type epidermis (E) mutant skin showed frequent fissures (F). Bars, 20 μm (A, B, and G); 10 μm (C–F, and H). s.b., s. basale.

always found in the posterior back and in several cases along the spine and on the forehead.

Premature and Increased Formation of Keratohyaline Granules and a Fragile Stratum Corneum in Cx43K258stop Epidermis

Compared with wild-type epidermis (Figure 4A), HE-stained sections showed significantly more and larger keratohyaline granules in the stratum(s). granulosum of Cx43K258stop mice (Figure 4B). The s. corneum of Cx43K258stop mice seemed to consist of more layers of thinner corneocytes (Figure 4B). TEM analysis provided further evidence for the premature occurrence of keratohyaline granules (white asterisk) in keratinocytes of the s. spinosum of Cx43K258stop mice (Figure 4D), and TEM and SEM confirmed the described increase in number but decrease in thickness (Figure 4D, black asterisk) of

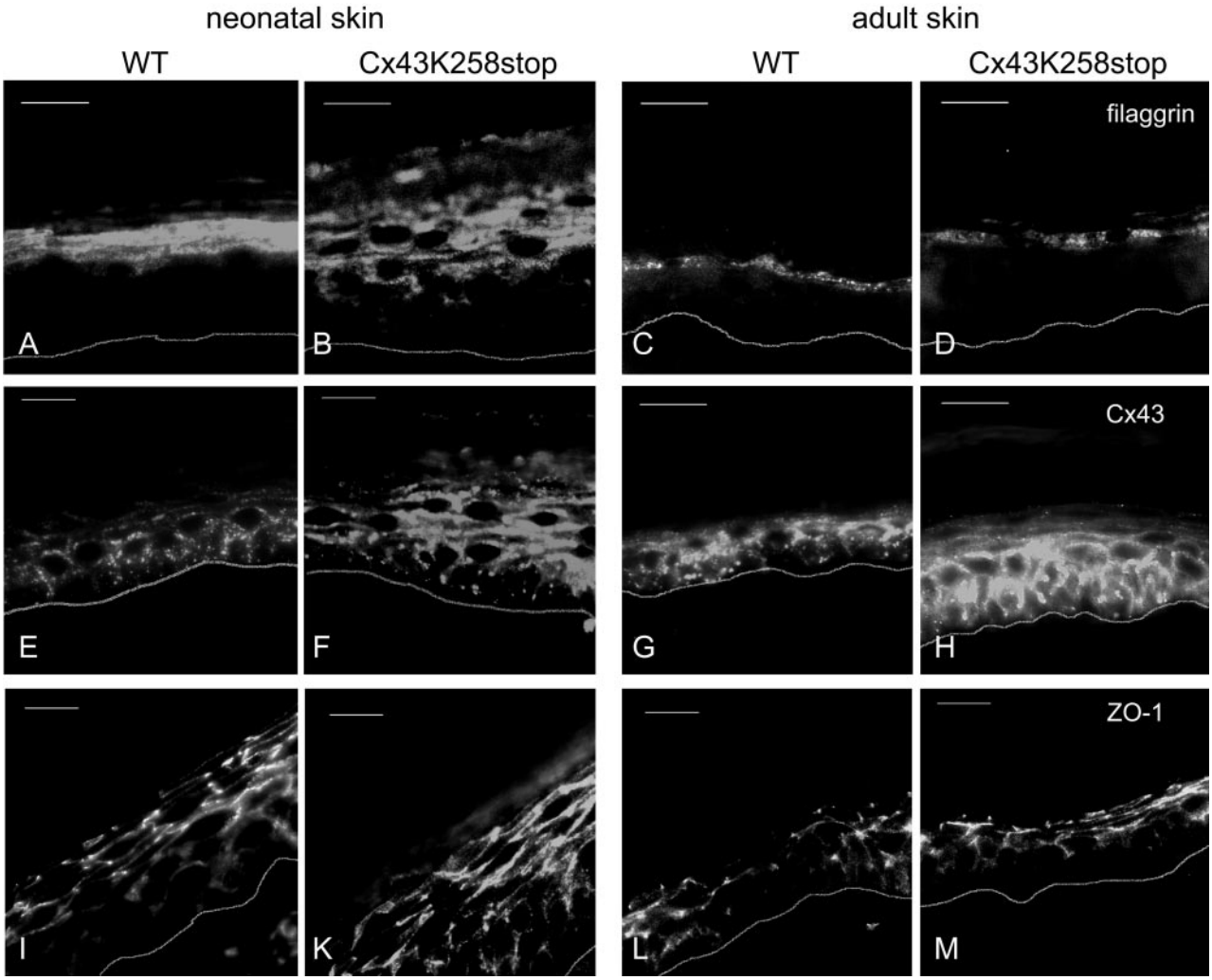

Figure 5. Immunofluorescence analysis of filaggrin, ZO-1, and Cx43 in epidermis. Cryosections of neonatal and adult epidermis of wild-type (A, C, E, G, I, and L) and homozygous Cx43K258stop animals (B, D, F, H, K, and M) were immunolabeled and the epidermis–dermis boundary was indicated by a white line. (A–D) Filaggrin was additionally detected in s. spinosum of neonatal homozygous Cx43K258stop animals (B). (E–H) In comparison with Cx43 (E and G), Cx43K258stop protein was abundantly expressed throughout neonatal homozygous mutant epidermis (K). In adult Cx43K258stop epidermis, the expression was elevated and detected mainly in the suprabasal s. spinosum (M). (I–M) ZO-1 was slightly elevated in homozygous mutant epidermis (K and M). Bars, 20 μm.

corneocyte layers (Figure 4, D and H). SEM of whole mount epidermis (Figure 4, E–H) displayed pronounced differences of the upper surface of the s. corneum between wild-type (Figure 4, E and G) and homozygous epidermis (Figure 4, F and H). In contrast to the continuous surface of wild-type epidermis with single desquamating corneocytes, the homozygous mutant epidermis seemed brittle and fragile with numerous fissures spanning several layers of corneocytes (Figure 4F).

Immunofluorescence Analysis of Epidermal Markers of Differentiation

No differences in the expression of keratin5, keratin1, and loricrin between wild-type and mutant genotypes were detected (Supplemental Figure 1, A–F). Filaggrin (Figure 5, A–D), on the other hand, showed a changed expression in neonatal, homozygous mutant epidermis. Whereas filaggrin was only detected in s. granulosum of wild-type neonatal epidermis (Figure 5A), labeling was found in one to two cell layers more basal in homozygous Cx43K258stop epidermis (Figure 5B), corresponding to the data obtained by TEM. Immunofluorescence analysis of adult epidermis revealed no persistence of the difference in the expression of filaggrin between wild-type and homozygous Cx43K258stop epidermis (Figure 5, C and D).

Immunofluorescence Analysis of ZO-1 and Connexin Expression in Neonatal Epidermis

Cx43 and Cx43K258stop protein expression (Figure 5, E–H) showed a significant difference between genotypes. Whereas Cx43 was restricted to s. basale and the lower layers of s. spinosum in wild-type neonatal (Figure 5E) and adult epidermis (Figure 5G), Cx43K258stop protein was found throughout the epidermis at a significantly elevated level in Cx43K258stop neonates (Figure 5F) and in adult homozygous mutant animals (Figure 5H). The tight junction protein ZO-1 (Figure 5, I–M) was located to s. granulosum and s. spinosum in both wild-type and mutant epidermis, with a slight increase in Cx43K258stop epidermis (Figure 5, K and

M). Analysis of other connexins expressed in epidermis revealed an up-regulation of Cx26 (Supplemental Figure 2, A and B), but no change in Cx30 and Cx31 expression (Supplemental Figure 2, C–F) in homozygous mutant epidermis. Analysis of proliferation and transition time of keratinocytes by 5-bromo-2-deoxyuridine (BrdU) labeling showed no differences between wild-type and Cx43K258stop epidermis (Supplemental Figure 1, I–M).

Changes in Filaggrin Processing and Connexin Expression in Neonatal Epidermis

During terminal differentiation, high-molecular-weight profilaggrin is proteolytically processed to monomeric filaggrin that associates with keratin filaments. Western blot analyses revealed no difference in total filaggrin expression, but at postnatal day 1 (Figure 6A), lower amounts of fully processed filaggrin (double asterisk) and an increase in the intermediate corresponding to three filaggrin domains (single asterisk) were noted. Analysis of connexin expression confirmed that the amount of Cx43K258stop protein expressed in neonatal, homozygous Cx43K258stop epidermis (Figure 6B, middle) was significantly higher than that of Cx43 protein expressed in wild-type littermates (Figure 6B, top). Whereas Cx26 protein was hardly detectable in wild-type neonatal epidermis, the expression was elevated in Cx43K258stop neonates (Figure 6B, bottom).

Cx43K258stop Protein Has a Prolonged Half-Life Time

Because Northern blot analyses of neonatal epidermis had shown no increase in *cx43K258stop* transcript (unpublished data), the increase in Cx43K258stop protein relative to Cx43 protein was apparently due to a difference in protein turnover. To determine the half-life time of the mutant Cx43 isoform, HeLa cell transfectants (Supplemental Figure, 3 A–F) were used. Whereas wild-type Cx43 (Figure 6C, top) showed the half-life time of 2.0 h as published for cultured cells (Laird *et al.*, 1991a), the life span of Cx43K258stop protein was more than doubled to 4.2 h (Figure 6C, bottom).

Cx43K258 Ovaries Display Abnormalities in Folliculogenesis

In contrast to adult wild-type ovaries (Figure 7, A–D), histological analysis of Cx43K258stop females revealed a strong impairment of folliculogenesis, mostly arrested at the antral stage (Figure 7, E–F). Rifts occurred between the follicular epithelial cells of late secondary oocytes leading to a cracked appearance (Figure 7F, arrow). In addition, immature follicles showed morphological abnormalities and often degenerating oocytes leading to ovarian cysts at the cortical surface of the ovary (Figure 7, E and F). Corpora lutea seemed not to develop from ovulation, because no corpora rubra could be observed. Instead, luteinization seemed to start already from immature antral follicles, as luteinized cells (Figure 7G, arrow) were observed in the center of follicles filled with follicular epithelial cells indicating a premature luteinization without preceding ovulation (Figure 7, G and H). In accordance, females carrying two Cx43K258stop alleles are infertile.

Histological Analysis of Cx43K258 Hearts

Histological investigations revealed that homozygous mutant hearts did not resemble the phenotype of Cx43 knockout mice. No obstruction of the right ventricular outflow tract, leading to the lethal phenotype of Cx43-deficient mice, was detected (Figure 8, A and B). Compared with hearts of wild-type littermates (Figure 8C), hearts of neonatal homozygous animals (Figure 8D) were smaller and typically had a bulb shape. The left ventricle was dilated apically. In the depicted homozygous heart, a persistent foramen ovale was found, but this was not seen in older animals. Preliminary analysis of adult hearts of surviving animals by echo-

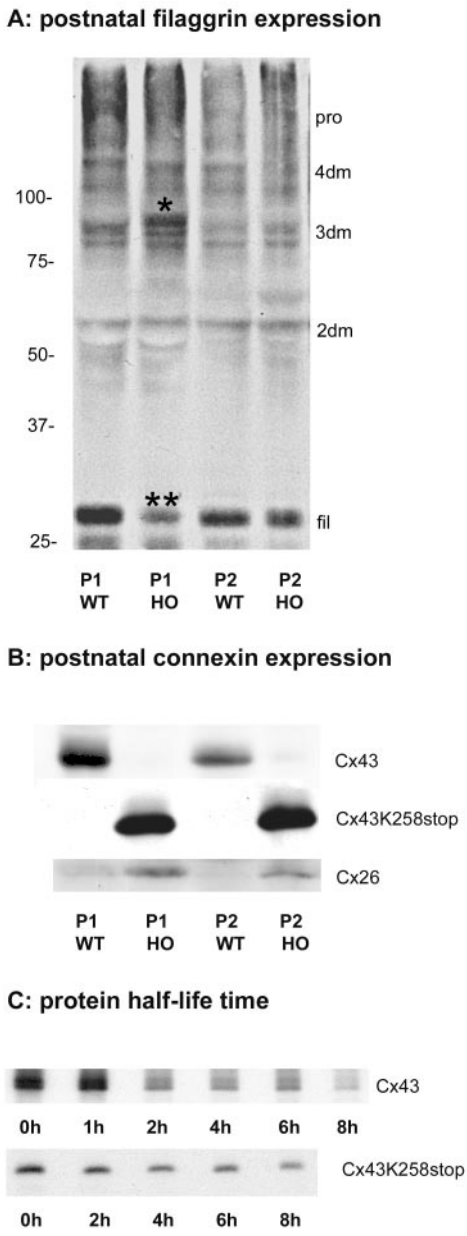

Figure 6. Immunoblot analyses of postnatal epidermis and Cx43K258stop protein turnover time in cultured HeLa cells. Immunoblot analysis (A and B) was carried out at postnatal days P1 (lanes 1 and 2) and P2 (lanes 3 and 4) of WT and HO epidermis. Amount of monumeric filaggrin was reduced in P1 homozygous epidermis (**), and an additional signal of higher molecular mass than the intermediate with three filaggrin domains (*) was found. Pro, profilaggrin; 4dm-2dm, intermediates with four, three, or two filaggrin domains; fil, monumeric filaggrin. (B) Membrane subsequently probed with primary antibodies to the cytoplasmic loop of Cx43 or to Cx26. Cx43K258stop and Cx26 amounts were elevated in homozygous epidermis. (C) Pulse-chase analyses on HeLa-Cx43WT and HeLa-Cx43K258stop cells revealed that the half-life time of Cx43K258stop was more than doubled to 4.2 h in comparison with 2.0 h for Cx43.

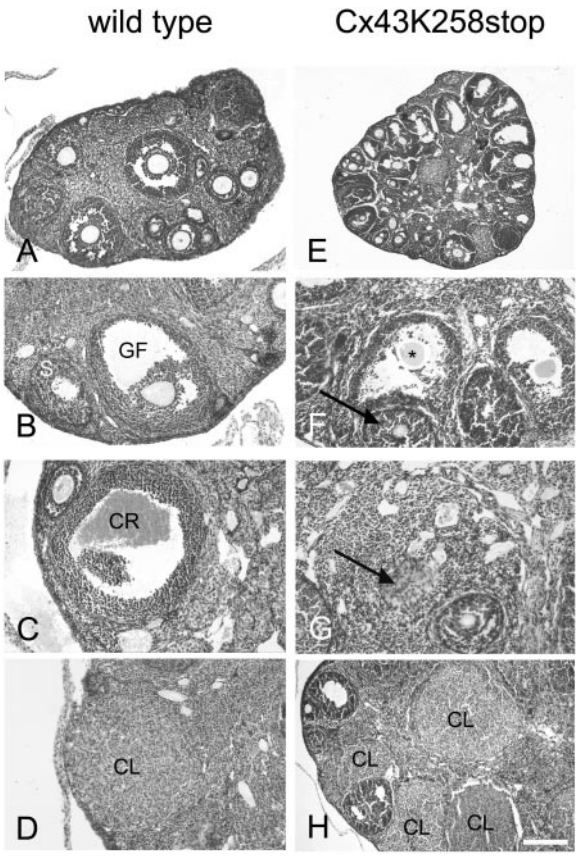

Figure 7. Histology of adult Cx43K258stop ovaries. (A–D) Normal folliculogenesis in wild-type ovaries (A and B), with ovulation indicated by formation of corpus rubrum (C) and subsequent development of corpora lutea (D). (E–H) In Cx43K258stop mice, follicular stages up to young Graafian follicles were observed, but no mature Graafian follicles developed (E). Preovulatory follicles showed morphological abnormalities (F, arrows) and degenerating oocytes (F, asterisk). Inappropriate luteinization (G) and corpora lutea formation without ovulation were observed (H). S, secondary follicle; GF, Graafian follicle; CR, corpus rubrum; CL, corpus luteum. Bars, 250 μm (A); 150 μm (B, C, D, F, and G); 375 μm (E); and 100 μm (H).

cardiography revealed functional impairment of the left ventricle (Videos 1–3). A heart with highly hypertrophic left ventricle showed contacting walls in systole and thereby reduced endsystolic volume (Video 2). On the other hand, a bulb-shaped heart with drastic dilatation was found in an adult homozygous animal (Video 3). This bulb-shaped heart displayed hypokinesis near the base of the heart and akinesis of the remaining ventricle. The endsystolic volume of the left ventricle was thereby drastically elevated. This heart very much resembled the histological findings of neonatal homozygous Cx43K258stop animals.

Electrocardiography of Neonatal Animals

In total, 144 mouse recordings were performed, i.e., 33 of Cx43 wild-type (WT), 71 of Cx43K258stop heterozygous (HT), and 40 of Cx43K258stop homozygous (HO) neonatal mice. Heart rate was 475 ± 61 beats per minute (bpm) in wild-type, 470 ± 60 bpm in heterozygous, and 424 ± 71 bpm in homozygous Cx43K258stop mice, indicating a significantly lower rate in homozygous mutant mice ($p < 0.001$). P-wave duration (WT, 15 ± 4 ms; HT, 14 ± 2 ms; and HO, 15 ± 4 ms), PQ-interval (WT, 43 ± 8 ms; HT, 41 ± 7 ms; and HO, 45 ± 9 ms), and QRS duration (WT, 16 ± 3 ms; HT, 16 ± 3 ms; and HO, 16 ± 4 ms) did not exhibit significant differences among the groups. QT-intervals could not be determined in 26 of 144 recordings due to artifacts with nonanalyzable ECGs equally distributed among all groups. Frequency-corrected QT-intervals (QT_c) demonstrated a significant longer repolarization in homozygous Cx43K258stop mice (WT, 19 ± 2 ms; HT, 21 ± 3 ms; and HO, 29 ± 17 ms; $p < 0.001$). (Figure 8G). However, subgroup analysis revealed that only seven homozygous Cx43K258stop mice demonstrated QT-prolongation along with significant ST- and T-elevation (Figure 8F; see HO_b in Figure 8G). The remaining 33 recordings of homozygous mice demonstrated a "normal" mean QT_c-interval and ST- and T-wave (Figure 8E; see HO_a in Figure 8G). No cardiac arrhythmias were documented. ECG parameters were compared between the three genotypes by means of one-way ANOVA and post hoc Tukey-Kramer multiple comparisons test. Unpaired Student's *t* test was performed for differentiation within a genotype. P values <0.05 were considered significant.

Analysis of Cx43 and ZO-1 Expression in Neonatal and Adult Hearts

Compared with the Cx43 expression in hearts of neonatal wild-type mice (Figure 9A), immunofluorescence analysis revealed elevated expression of Cx43K258stop protein (Figure 9B) in homozygous mutant hearts. The difference was most prominent in the epicardial region of the ventricle. Western blot analyses of neonatal hearts confirmed overall increase of Cx43K258stop protein (unpublished data). Immunofluorescence analysis of adult hearts revealed similar amounts of Cx43/Cx43K258stop protein (Figure 9, C and D), the Cx43 isoforms located in the intercalated discs in both genotypes. ZO-1 showed a slight up-regulation in homozygous Cx43K258stop hearts (Figure 9, E–F). In adult hearts, ZO-1 protein (Figure 9, G and H) was found in intercalated discs in both genotypes.

Mice Harboring One cx43K258stop and One cx43KO Allele Show a Rescue of the Epidermal Abnormalities

Analyses of the offspring of crossings of heterozygous Cx43K258stop mice to transgenic mice harboring one deleted *cx43* allele (Theis *et al.*, 2001) surprisingly revealed that the observed epidermal phenotype was dependent on the *cx43K258stop* gene dosage. Whereas <3% of all born homozygous Cx43K258stop mice survived to adulthood (Figure 10 A), >50% of mice harboring one *cx43K258stop* and one *cx43KO* allele reached adulthood (Figure 10B). The dye penetration assay with toluidine blue revealed that these mice did not exhibit an epidermal barrier defect (Figure 10D).

DISCUSSION

To analyze the function of the C-terminal region of Cx43 in vivo, we replaced endogenous Cx43 by Cx43K258stop in mice. This mutation resulted in a premature stop codon leading to the expression of a Cx43 isoform that lacks the last 125 amino acid residues of the cytoplasmic C-terminal domain but still forms functional gap junctional channels when expressed in *Xenopus* oocytes (Morley *et al.*, 1996) or mouse 3T3 cells (Moorby and Gherardi, 1999).

Homozygous Cx43K258stop animals were born at the expected frequency, and newborns were per se viable, indicating that the mutant Cx43 surprisingly does not grossly impair normal embryonic development. Postnatal, homozy-

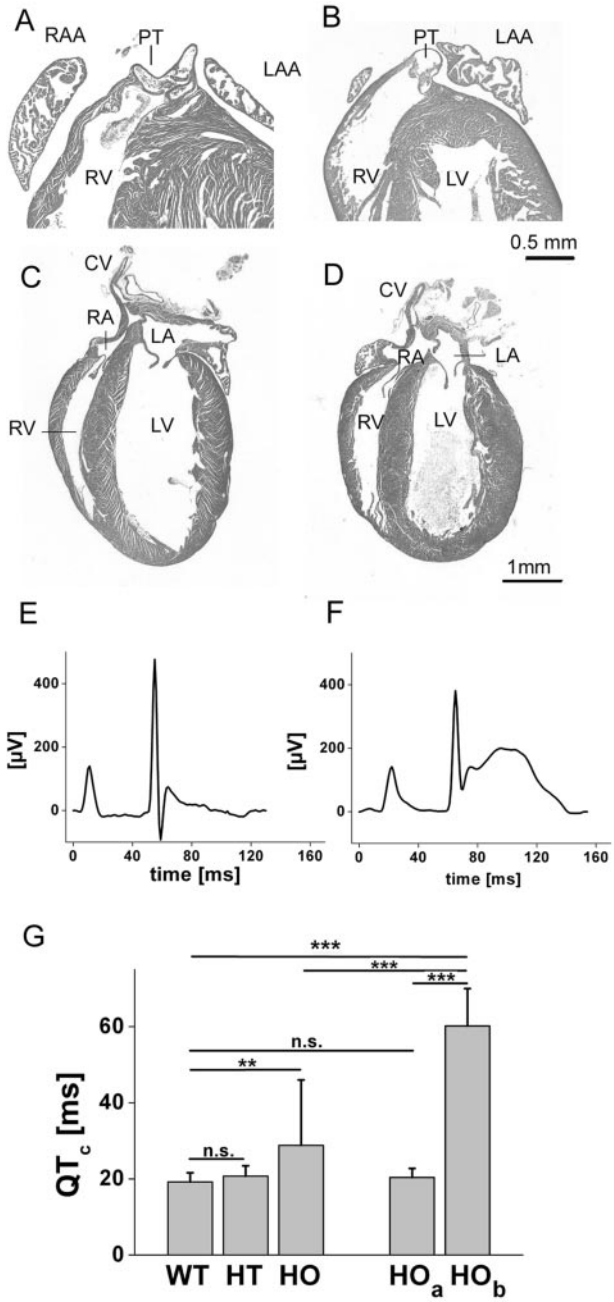

Figure 8. Histology and electrocardiography of neonatal Cx43K258stop hearts. (A–D) HE-stained sections of neonatal wild-type (A and C) and homozygous Cx43K258stop (B and D) hearts. The subpulmonary outlet of the Cx43K258stop heart (B) is normally open as that of the wild type (A). Cx43K258stop hearts (D) have a bulb shape with a dilated left ventricle and blunt apex. CV, caval vein; RA, right atrium; RV, right ventricle; LA, left atrium; LV, left ventricle; PT, pulmonary truncus; RAA, right atrial appendage; LAA, left atrial appendage. Bars, 500 μm (A and B); and 1 mm (C and D). (E and F) Signal-averaged ECG recordings of two homozygously mutated pups on postnatal day 2; the animal in E showed an unobtrusive ECG, whereas the animal in F displayed ST-elevation, QT-prolongation, and enlarged T-wave. (G) Frequency-corrected QT_c-intervals demonstrated a significant longer repolarization in homozygous Cx43K258stop mice. The high SD in QT_c of homozygous mice is explained by a subgroup of seven mice (HO_b) demonstrating a significantly higher QT_c compared with wild type (E, 60 $\pm$ 10 ms; $p < 0.001$). Remaining ($n = 33$) pups in this group (Ho_a) demonstrated no differences to WT or HT. n.s., $p > 0.05$; **$p < 0.01$; ***$p < 0.001$.

gous Cx43K258stop mice were largely lethal, i.e., <3% survived to adulthood. Here, we show that lethality of homozygous Cx43K258stop mice is caused by a defective epidermal permeability barrier. This barrier is formed by terminally differentiated keratinocytes and lipids and is crucial for survival ex utero, because it retards dehydration and inhibits invasion of microorganisms and noxious material (Cartlidge, 2000). Defects of the epidermal permeability barrier in mice are related to mutations of genes involved in terminal differentiation of keratinocytes (Segre, 2003). Most of these animals die within the first 2 d, due to a complete loss of the epidermal permeability barrier. Animals displaying only punctuate epidermal permeability barrier defects such as mice with ablated desmocollin-1 (Chidgey *et al.*, 2001) survive to adulthood. The fact that loss of the epidermal permeability barrier in Cx43K258stop mice does not affect the complete body surface explains why not all of these mice die during the first week. At the molecular level of neonatal epidermis, an elevated level and altered expression pattern of Cx43K258stop compared with wild-type Cx43 protein, an up-regulation of Cx26 and ZO-1, and a broader expression of filaggrin, together with changes in the processing of this protein, were detected. Only filaggrin was normally reexpressed in the small subset of surviving animals. Similarly, mice overexpressing claudin-6 (Turksen and Troy, 2002) and exhibiting defective epidermal permeability barrier, also showed a broader expression and altered processing of filaggrin. How can the mutant Cx43 protein lead to the observed phenotype? During embryogenesis, the epidermal expression pattern of connexins changes (Choudhry *et al.*, 1997), whereas Cx43 and Cx26 are coexpressed in the suprabasal and basal layers between embryonic day 12 and 15, Cx26 becomes restricted to s. granulosum, whereas Cx43 is only found in the basal and suprabasal layers from day 17 of embryogenesis onwards. This is the time when the epidermal permeability barrier begins to cover the body surface. The switch in gap junction protein expression has been postulated to be associated with selective changes in gap junctional channel permeability during keratinocyte differentiation (Brissette *et al.*, 1994). Cx43K258stop protein displayed a prolonged half-life time. This is in accordance with data on human Cx43 by Thomas *et al.* (2003), showing increased Cx43 half-life of 2–6 h when residue tyrosine 286 was mutated. The persistence of mutant Cx43 gap junction channels in the upper layers of the epidermis seems to interfere with terminal kerationcyte differentiation and complete closure of the epidermal permeability barrier before birth. Presumably, the calcium-dependent shift from a broad to a narrow epidermal expression pattern of Cx43 (Brissette *et al.*, 1994) cannot be achieved in time due to the prolonged turnover of Cx43K258stop protein. Interestingly, recently generated mice harboring one *cx43K258stop* and one *cx43knockout* allele do not suffer from a defective epidermal barrier and >50% of these mice survive to adulthood. This implies that the epidermal phenotype is dependent on the dosage of the *cx43K258stop* gene. The presence of large amounts of mutant Cx43K258stop protein in differentiated keratinocytes apparently impairs establishment of the precisely adjusted calcium gradient across the epidermis that is crucial for keratinocyte differentiation and homeostasis of the epidermal barrier (Elias *et al.*, 1998, 2002). The observed changes in filaggrin expression and processing are in line with this conclusion, because these steps are dependent on calcium (Resing *et al.*, 1993). Filaggrin not only has the function of bundling keratins in corneocytes but also subsequently is degraded to modified free amino acids in s. corneum. These modified amino acids are highly hygroscopic

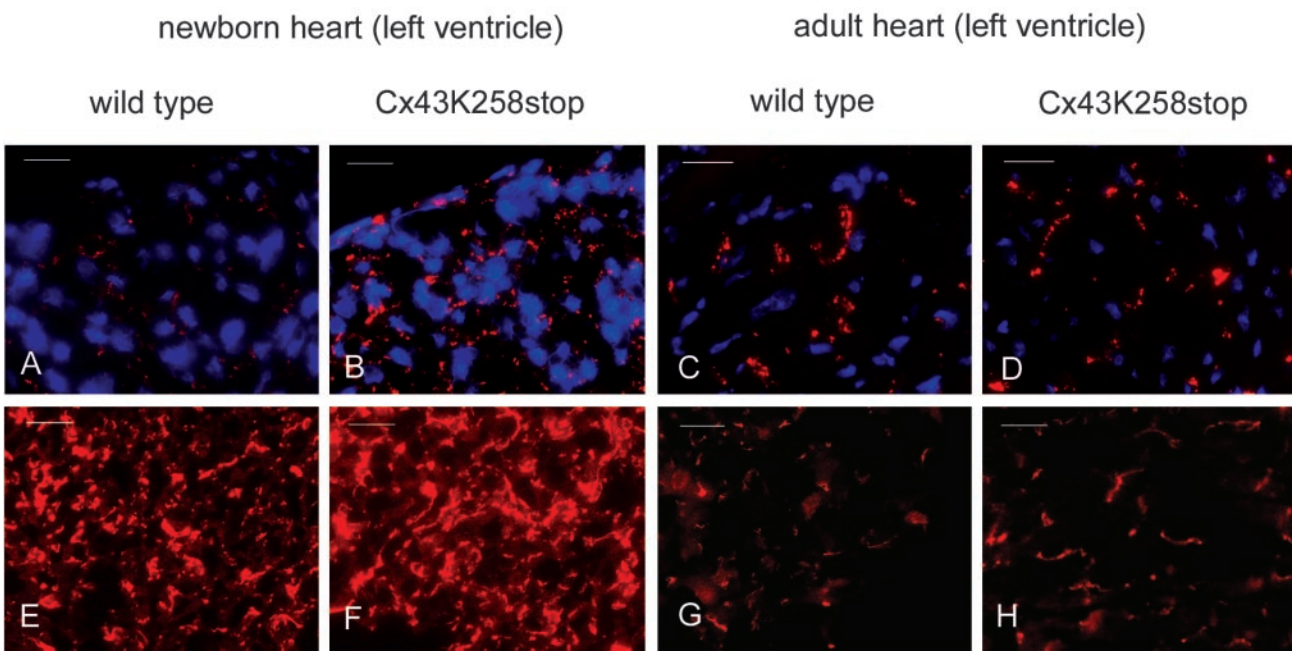

Figure 9. Immunofluorescence analysis of hearts. Cryosections of neonatal (A, B, E, and F) and adult hearts (C, D, G, and H) were immunolabeled and costained for nuclei. (A–D) Compared with neonatal wild type (A), Cx43K258stop immunoreactive spots in the epicardial region of neonatal homozygous left ventricle (B) were increased in size. In adults, Cx43 and Cx43K258stop were detectable in intercalated discs in both genotypes (C and D). (E–H) ZO-1 expression was slightly elevated in homozygous mutant Cx43K258stop hearts (F and H). Bars, 20 μm.

and essential for maintaining osmolarity and flexibility of the epidermis (Rawlings *et al.*, 1994; Elias, 2004). Delay in full filaggrin processing and subsequent shortage in hygroscopic amino acid residues in corneocytes could explain the thinness and fragility of corneocytes seen in Cx43K258stop epidermis. Future analysis regarding lamellar bodies production and secretion, and activity of transglutaminases and lipid-modifying enzymes will help to clarify whether

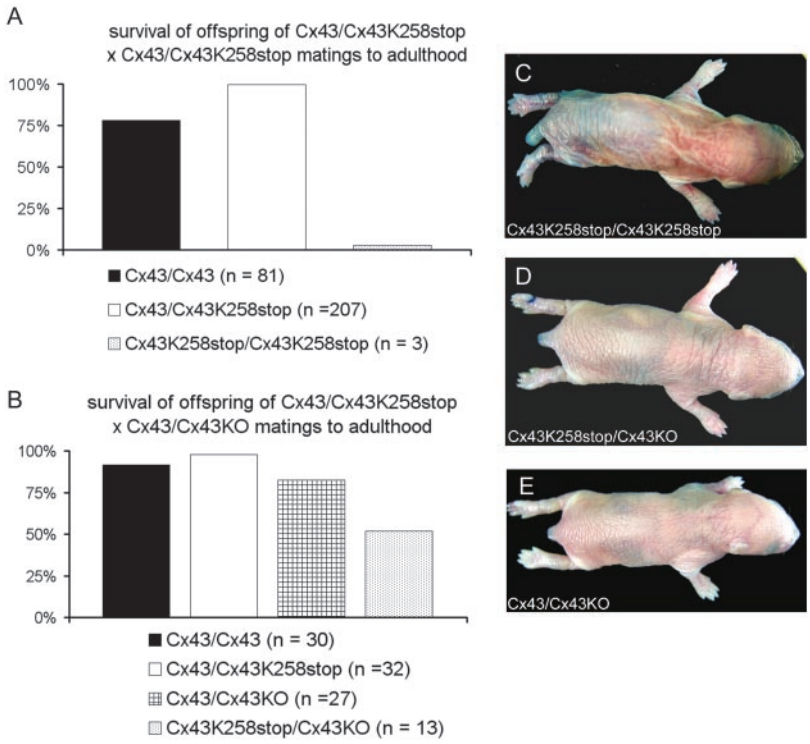

Figure 10. Cx43K258stop gene dosage influences epidermal phenotype and postnatal survival. Postweaning offspring was grouped according to genotypes. (A) Only 311 of 415 born animals from heterozygous Cx43WT/Cx43K258stop matings survived to adulthood. According to the expected Mendelian ratio of 50% heterozygous and both 25% wild-type and homozygous animals, percentages of survival were multiplied by 2 or 4, respectively. Less than 3% of all expected homozygous animals survived to adulthood. (B) Animals (105 of 131) from Cx43WT/Cx43K258stop × Cx43K258stop/Cx43KO matings survived to adulthood. According to the Mendelian ratio of each 25% Cx43/Cx43, Cx43WT/Cx43K258stop, Cx43K258stop/Cx43KO, and Cx43K258stop/Cx43KO animals, percentages of survival were multiplied by 4 to determin general survival percentage of the different groups. Cx43/Cx43, Cx43/Cx43K258stop, and Cx43/Cx43KO displayed survival in the range between 75 and 100%. Whereas Cx43K258stop/Cx43KO animals still displayed a reduced survival, >16 times as many animals of this genotype reached adulthood compared with homozygous Cx43K258stop animals. (C–E) In contrast to homozygous neonatal Cx43K258stop animals (C), toluidine dye penetration assay revealed no staining due to a defective barrier in Cx43K258stop/Cx43KO (D) and Cx43/Cx43KO (E) animals.

other steps in permeability barrier development and maintenance also are impaired in homozygous Cx43K258 stop neonates.

The occurrence of constriction rings around the tails of homozygous Cx43K258stop mice, in some cases leading to autoamputation, was reminiscent of human Vohwinkel's disease. Vohwinkel's disease has been linked to mutations in the *loricrin* and *cx26* genes (Korge *et al.*, 1997; van Steensel *et al.*, 2002). Mice expressing mutated loricrin or Cx26 protein model the phenotype of this disease (Suga *et al.*, 2000; Bakirtzis *et al.*, 2003). In comparison with wild-type littermates, tails of homozygous Cx43K258stop neonates showed a completely smooth surface in preliminary SEM analysis with no signs of desquamation. The very compact s. corneum locally invaginated and led to the observed constriction rings. A similar phenotype was documented by Bakirtzis *et al.* (2003) in mice expressing mutant Cx26 (Cx26D66H). Recent analysis of s. corneum functions in human patients suffering from the loricrin linked form of Vohwinkel disease also attributed the abnormalities to impairments of the epidermal permeability barrier accompanied by defects in desquamation and the occurrence of corneocytic fragility (Schmuth *et al.*, 2004).

Regarding the oculodentodigital dysplasia (ODDD) disease that has been linked to mutations of the *cx43* gene in humans, only a mild epidermal phenotype was so far described in one patient (Paznekas *et al.*, 2003). One reason why the ODDD mutations might not lead to epidermal abnormalities could be the difference in the epidermal expression patterns of Cx26 and Cx43 between mouse and human. In addition, mutations mapped to ODDD were never found within the C-terminal region of Cx43. This could imply that ODDD mutations rather change the permeability or per se coupling possibility of Cx43 gap junction channels, whereas the Cx43K258stop mutation mainly influences gating regulation and stability of Cx43. Maybe a similar mutation in the human genome is not tolerable during embryogenesis, pointing to a harsher phenotype due to misregulated Cx43 than to changes in channel permeability. This could also be the reason that (so far) no mutations in the C-terminal domain of Cx43 have been found associated with ODDD.

Homozygous Cx43K258stop females that survive to adulthood were infertile. Histological analysis revealed that Cx43K258stop protein impaired antral stage formation in folliculogenesis, and corpora lutea formation occurred without ovulation. Interestingly, these findings rather resemble the ovarian phenotype seen in Cx37-deficient mice than the impairments in folliculogenesis in Cx43-deficient ovaries. Only Cx37 is expressed in the oocyte (Kidder and Mhawi, 2002), whereas granulosa cells express different gap junction isoforms, including Cx43. Simon *et al.* (1997) showed, that Cx37 deficient mice lack mature Graafian follicles and develop numerous incomplete corpora lutea. Loss of Cx43 on the other hand resulted in an arrest of follicular growth, with most follicles failing to develop multiple granulosa cell layers characteristic of secondary follicles (Ackert *et al.*, 2001; Gittens *et al.*, 2003). This implies that the presence of Cx37 and functional regulation and/or turnover of Cx43 are necessary for ovulation in late folliculogenesis. The findings are in accordance with the observed change in phosphorylation and subsequent decrease of the Cx43 protein that follow stimulation by luteinizing hormone in late folliculogenesis (Granot and Dekel, 1998).

Homozygous Cx43K258stop neonates displayed bulb-formed hearts and were different from the phenotype of mice with generally ablated Cx43 (Reaume *et al.*, 1995). No obstructions of the right ventricular outflow tract due to the formation of trabecular pouches were found. The bulb shape of neonatal hearts together with preliminary data obtained from echocardiograms of adult homozygous Cx43K258stop hearts pointed to persisting left ventricular dysfunction. This is most likely due to mutual influences of changes in cardiomyocyte architecture and electrophysiological properties. Perinatally, Cx43 and calcium-dependent cell contact proteins, including ZO-1, are dispersed around the sarcolemma of cardiomyocytes (Barker *et al.*, 2002) before intercalated discs begin to form. To date, there are two possible explanations for this transition. First, there could be a different turnover rate of Cx43 in different parts of the myocyte (Saffitz *et al.*, 2000) and the detected prolonged half-life time of Cx43K258stop could therefore account for disturbed formation of functional myocyte architecture. Second, Cx43 might be positioned at the intercalated discs by direct interactions with cytoskeleton proteins (Toyofuku *et al.*, 1998). Because the Cx43K258stop mutation also deletes the interaction site for ZO-1, this mechanism also would be impaired. However, in the small subset of Cx43K258stop animals surviving to adulthood, analysis of their hearts for ZO-1 and Cx43K258stop expression revealed the typical staining pattern of intercalated discs for both proteins, implying that both proteins finally can reach their destination in cardiomyocytes without direct interaction.

The detected atrioseptal defect in a homozygous Cx43K258stop neonate was in accordance with the findings that Cx43 takes part in murine atrial septation (Kirchhoff *et al.*, 2000; Lo, 2000). In humans, two families suffering from ODDD were reported that suffer cardiac abnormalities, and one patient with the Cx43G21R mutation showed an atrioseptal defect (Paznekas *et al.*, 2003). Before mapping of the *cx43* ODDD mutations, a phenotypic link between ODDD and heart septation defects was described previously (Schneider *et al.*, 1977; Judisch *et al.*, 1979).

Our main electrophysiological finding was a QT-prolongation, in combination with a T-wave elevation, in ~20% of neonatal Cx43K258stop mice. The relative change in transmural distribution of Cx43K258stop protein in comparison with Cx43 protein together with the presumed delay in formation of intercalated discs, might cause inhomogeneous and delayed repolarization. Similar ECG abnormalities with ST-elevation and QT-prolongation as an overlap of Brugada- and Long-QT-syndrome have been described in association with mutations in the *SCN5A* sodium channel gene (Priori *et al.*, 2000; Rivolta *et al.*, 2001). Interestingly, the elevation of the ST-segment typical for the Brugada syndrome is explained by a changed transmural voltage gradient caused by an abbreviation of epicardial action potential duration (Yan and Antzelevitch, 1999). Thus, the accumulation of Cx43K258stop and impairment in its colocalization with sodium channels in intercalated discs (Kucera *et al.*, 2002) could provide a potential explanation for the repolarization abnormalities found.

In summary, the high postnatal lethality of homozygous Cx43K258stop mice was correlated to a defective epidermal permeability barrier. Less than 1% of all animals survived to adulthood. Surviving female animals were infertile due to a defective folliculogenesis reminiscent of the Cx37 knockout phenotype. In surviving adult mice, the defects in the epidermal permeability barrier were rescued, but they still displayed cardiac dysfunction of the left ventricle. Primary cardiomyocyte cultures and detailed electrophysiological and histological analyses of the hearts of surviving Cx43K258stop mice should help to clarify the mechanisms

leading to the observed cardiac changes due to the truncation of Cx43.

ACKNOWLEDGMENTS

We thank Drs. Peter Nielsen and Nalin Kumar (Scripps Research Institute, La Jolla, CA) for a sample of antibodies directed to the cytoplasmic loop of Cx43 (Yeager and Gilula, 1992). We gratefully acknowledge the technical help of Ina Fiedler and Gaby Schwarz. This work was supported by grants of the German Research Association (SFB 284, C1, Wi 270/25-1,2) and the research group on "keratinocytes" to K.W.

REFERENCES

Ackert, C.L., Gittens, J.E., O'Brien, M.J., Eppig, J.J., and Kidder, G.M. (2001). Intercellular communication via connexin43 gap junctions is required for ovarian folliculogenesis in the mouse. Dev. Biol. *233*, 258–270.

Bakirtzis, G., *et al*. (2003). Targeted epidermal expression of mutant Connexin 26(D66H) mimics true Vohwinkel syndrome and provides a model for the pathogenesis of dominant connexin disorders. Hum. Mol. Genet. *12*, 1737–1744.

Barker, R.J., Price, R.L., and Gourdie, R.G. (2002). Increased association of ZO-1 with connexin43 during remodeling of cardiac gap junctions. Circ. Res. *90*, 317–324.

Brissette, J.L., Kumar, N.M., Gilula, N.B., Hall, J.E., and Dotto, G.P. (1994). Switch in gap junction protein expression is associated with selective changes in junctional permeability during keratinocyte differentiation. Proc. Natl. Acad. Sci. USA *91*, 6453–6457.

Cartlidge, P. (2000). The epidermal barrier. Semin. Neonatol. *5*, 273–280.

Chidgey, M., *et al*. (2001). Mice lacking desmocollin 1 show epidermal fragility accompanied by barrier defects and abnormal differentiation. J. Cell Biol. *155*, 821–832.

Choudhry, R., Pitts, J.D., and Hodgins, M.B. (1997). Changing patterns of gap junctional intercellular communication and connexin distribution in mouse epidermis and hair follicles during embryonic development. Dev. Dyn. *210*, 417–430.

Dasgupta, C., A.M. Martinez, C.W. Zuppan, M.M. Shah, L.L. Bailey, and W.H. Fletcher. 2001. Identification of connexin43 (alpha1) gap junction gene mutations in patients with hypoplastic left heart syndrome by denaturing gradient gel electrophoresis (DGGE). Mutat. Res. *479*, 173–186.

Delmar, M., Coombs, W., Sorgen, P., Duffy, H.S., and Taffet, S.M. (2004). Structural bases for the chemical regulation of Connexin43 channels. Cardiovasc. Res. *62*, 268–275.

Duffy, H.S., Sorgen, P.L., Girvin, M.E., O'Donnell, P., Coombs, W., Taffet, S.M., Delmar, M., and Spray, D.C. (2002). pH-dependent intramolecular binding and structure involving Cx43 cytoplasmic domains. J. Biol. Chem. *277*, 36706–36714.

Elias, P.M. (2004). The epidermal permeability barrier: from the early days at Harvard to emerging concepts. J. Investig. Dermatol. *122*, 36–39.

Elias, P.M., Ahn, S.K., Denda, M., Brown, B.E., Crumrine, D., Kimutai, L.K., Komuves, L., Lee, S.H., and Feingold, K.R. (2002). Modulations in epidermal calcium regulate the expression of differentiation-specific markers. J. Investig. Dermatol. *119*, 1128–1136.

Elias, P.M., Nau, P., Hanley, K., Cullander, C., Crumrine, D., Bench, G., Sideras-Haddad, E., Mauro, T., Williams, M.L., and Feingold, K.R. (1998). Formation of the epidermal calcium gradient coincides with key milestones of barrier ontogenesis in the rodent. J. Investig. Dermatol. *110*, 399–404.

Evans, W.H., and Martin, P.E. (2002). Lighting up gap junction channels in a flash. Bioessays *24*, 876–880.

Giepmans, B.N., Hengeveld, T., Postma, F.R., and Moolenaar, W.H. (2001a). Interaction of c-Src with gap junction protein connexin-43. Role in the regulation of cell-cell communication. J. Biol. Chem. *276*, 8544–8549.

Giepmans, B.N., and Moolenaar, W.H. (1998). The gap junction protein connexin43 interacts with the second PDZ domain of the zona occludens-1 protein. Curr. Biol. *8*, 931–934.

Giepmans, B.N., Verlaan, I., Hengeveld, T., Janssen, H., Calafat, J., Falk, M.M., and Moolenaar, W.H. (2001b). Gap junction protein connexin-43 interacts directly with microtubules. Curr. Biol. *11*, 1364–1368.

Gittens, J.E., Mhawi, A.A., Lidington, D., Ouellette, Y., and Kidder, G.M. (2003). Functional analysis of gap junctions in ovarian granulosa cells: distinct role for connexin43 in early stages of folliculogenesis. Am. J. Physiol. *284*, C880–C887.

Goldberg, G.S., Bechberger, J.F., and Naus, C.C. (1995). A pre-loading method of evaluating gap junctional communication by fluorescent dye transfer. Biotechniques *18*, 490–497.

Granot, I., and Dekel, N. (1998). Cell-to-cell communication in the ovarian follicle: developmental and hormonal regulation of the expression of connexin43. Hum. Reprod. *13* (suppl 4), 85–97.

Hagendorff, A., Schumacher, B., Kirchhoff, S., Lüderitz, B., and Willecke, K. (1999). Conduction disturbances and increased atrial vulnerability in Connexin40-deficient mice analyzed by transesophageal stimulation. Circulation *99*, 1508–1515.

Hardman, M.J., Sisi, P., Banbury, D.N., and Byrne, C. (1998). Patterned acquisition of skin barrier function during development. Development *125*, 1541–1552.

Harris, A.L. (2001). Emerging issues of connexin channels: biophysics fills the gap. Q. Rev. Biophys. *34*, 325–472.

Hertlein, B., Butterweck, A., Haubrich, S., Willecke, K., and Traub, O. (1998). Phosphorylated carboxy terminal serine residues stabilize the mouse gap junction protein connexin45 against degradation. J. Membr. Biol. *162*, 247–257.

Hogan B., Beddington R., Costantini F., and Lacy E. 1994. Manipulating the Mouse Embryo: A Laboratory Manual, Cold Spring Harbor, NY: Cold Spring Harbor Laboratory Press.

Homma, N., Alvarado, J.L., Coombs, W., Stergiopoulos, K., Taffet, S.M., Lau, A.F., and Delmar, M. (1998). A particle-receptor model for the insulin-induced closure of connexin43 channels. Circ. Res. *83*, 27–32.

Horst, E., Wijngaard, P.L., Metzelaar, M., Bast, E.J., and Clevers, H.C. (1991). A method for cDNA cloning in COS cells irrespective of subcellular site of expression. Nucleic Acids Res. *19*, 4556.

Judisch, G.F., Martin-Casals, A., Hanson, J.W., and Olin, W.H. (1979). Oculodentodigital dysplasia. Four new reports and a literature review. Arch. Ophthalmol. *97*, 878–884.

Kidder, G.M., and Mhawi, A.A. (2002). Gap junctions and ovarian folliculogenesis. Reproduction *123*, 613–620.

Kim, D.Y., Kam, Y., Koo, S.K., and Joe, C.O. (1999). Gating connexin 43 channels reconstituted in lipid vesicles by mitogen-activated protein kinase phosphorylation. J. Biol. Chem. *274*, 5581–5587.

Kirchhoff, S., Kim, J.S., Hagendorff, A., Thönnissen, E., Krüger, O., Lamers, W.H., and Willecke, K. (2000). Abnormal cardiac conduction and morphogenesis in connexin40 and connexin43 double-deficient mice. Circ. Res. *87*, 399–405.

Korge, B.P., Ishida-Yamamoto, A., Punter, C., Dopping-Hepenstal, P.J., Iizuka, H., Stephenson, A., Eady, R.A., and Munro, C.S. (1997). Loricrin mutation in Vohwinkel's keratoderma is unique to the variant with ichthyosis. J. Investig. Dermatol. *109*, 604–610.

Kucera, J.P., Rohr, S., and Rudy, Y. (2002). Localization of sodium channels in intercalated disks modulates cardiac conduction. Circ. Res. *91*, 1176–1182.

Laemmli, U.K. (1970). Cleavage of structural proteins during the assembly of the head of bacteriophage T4. Nature *227*, 680–685.

Laird, D.W., Puranam, K.L., and Revel, J.P. (1991a). Turnover and phosphorylation dynamics of connexin43 gap junction protein in cultured cardiac myocytes. Biochem. J. *273*, 67–72.

Laird, P.W., Zijderveld, A., Linders, K., Rudnicki, M.A., Jaenisch, R., and Berns, A. (1991b). Simplified mammalian DNA isolation procedure. Nucleic Acids Res. *19*, 4293.

Lampe, P.D., and Lau, A.F. (2000). Regulation of gap junctions by phosphorylation of connexins. Arch. Biochem. Biophys. *384*, 205–215.

Lampe, P.D., TenBroek, E.M., Burt, J.M., Kurata, W.E., Johnson, R.G., and Lau, A.F. (2000). Phosphorylation of connexin43 on serine368 by protein kinase C regulates gap junctional communication. J. Cell Biol. *149*, 1503–1512.

Liu, S., Taffet, S., Stoner, L., Delmar, M., Vallano, M.L., and Jalife, J. (1993). A structural basis for the unequal sensitivity of the major cardiac and liver gap junctions to intracellular acidification: the carboxyl tail length. Biophys. J. *64*, 1422–1433.

Lo, C.W. (2000). Role of gap junctions in cardiac conduction and development: insights from the connexin knockout mice. Circ. Res. *87*, 346–348.

Mitchell, G.F., Jeron, A., and Koren, G. (1998). Measurement of heart rate and Q-T interval in the conscious mouse. Am. J. Physiol. *274*, H747–H751.

Moorby, C.D., and Gherardi, E. (1999). Expression of a Cx43 deletion mutant in 3T3 A31 fibroblasts prevents PDGF-induced inhibition of cell communication and suppresses cell growth. Exp. Cell Res. *249*, 367–376.

Moreno, A.P., Chanson, M., Elenes, S., Anumonwo, J., Scerri, I., Gu, H., Taffet, S.M., and Delmar, M. (2002). Role of the carboxyl terminal of connexin43 in transjunctional fast voltage gating. Circ. Res. *90*, 450–457.

Morley, G.E., Taffet, S.M., and Delmar, M. (1996). Intramolecular interactions mediate pH regulation of connexin43 channels. Biophys. J. *70*, 1294–1302.

Musil, L.S., Cunningham, B.A., Edelman, G.M., and Goodenough, D.A. (1990). Differential phosphorylation of the gap junction protein connexin43 in junctional communication-competent and -deficient cell lines. J. Cell Biol. *111*, 2077–2088.

Niessen, H., Harz, H., Bedner, P., Kramer, K., and Willecke, K. (2000). Selective permeability of different connexin channels to the second messenger inositol 1,4,5-trisphosphate. J. Cell Sci. *113*, 1365–1372.

Paznekas, W.A., *et al*. (2003). Connexin 43 (GJA1) mutations cause the pleiotropic phenotype of oculodentodigital dysplasia. Am. J. Hum. Genet. *72*, 408–418.

Plum, A., *et al*. (2000). Unique and shared functions of different connexins in mice. Curr. Biol. *10*, 1083–1091.

Priori, S.G., *et al*. (2000). Clinical and genetic heterogeneity of right bundle branch block and S.T-segment elevation syndrome: a prospective evaluation of 52 families. Circulation *102*, 2509–2515.

Qu, Y., and Dahl, G. (2002). Function of the voltage gate of gap junction channels: selective exclusion of molecules. Proc. Natl. Acad. Sci. USA *99*, 697–702.

Rawlings, A.V., Scott, I.R., Harding, C.R., and Bowser, P.A. (1994). Stratum corneum moisturization at the molecular level. J. Investig. Dermatol. *103*, 731–741.

Reaume, A.G., de Sousa, P.A., Kulkarni, S., Langille, B.L., Zhu, D., Davies, T.C., Juneja, S.C., Kidder, G.M., and Rossant, J. (1995). Cardiac malformation in neonatal mice lacking connexin43. Science *267*, 1831–1834.

Resing, K.A., al Alawi, N., Blomquist, C., Fleckman, P., and Dale, B.A. (1993). Independent regulation of two cytoplasmic processing stages of the intermediate filament-associated protein filaggrin and role of Ca2+ in the second stage. J. Biol. Chem. *268*, 25139–25145.

Rivolta, I., Abriel, H., Tateyama, M., Liu, H., Memmi, M., Vardas, P., Napolitano, C., Priori, S.G., and Kass, R.S. (2001). Inherited Brugada and long QT-3 syndrome mutations of a single residue of the cardiac sodium channel confer distinct channel and clinical phenotypes. J. Biol. Chem. *276*, 30623–30630.

Saffitz, J.E., Laing, J.G., and Yamada, K.A. (2000). Connexin expression and turnover: implications for cardiac excitability. Circ. Res. *86*, 723–728.

Schmuth, M., *et al*. (2004). Structural and functional consequences of loricrin mutations in human loricrin keratoderma (Vohwinkel syndrome with ichthyosis). J. Investig. Dermatol. *122*, 909–922.

Schneider, J.A., Shaw, G.G., and Van Reken, D.E. (1977). Congenital heart disease in oculodentodigital dysplasia. Va Med. *104*, 262–263.

Segre, J. (2003). Complex redundancy to build a simple epidermal permeability barrier. Curr. Opin. Cell Biol. *15*, 776–782.

Simon, A.M., Goodenough, D.A., Li, E., and Paul, D.L. (1997). Female infertility in mice lacking connexin 37. Nature *385*, 525–529.

Söhl, G., and Willecke, K. (2003). An update on connexin genes and their nomenclature in mouse and man. Cell Commun. Adhes. *10*, 173–180.

Stacey, A., Schnieke, A., McWhir, J., Cooper, J., Colman, A., and Melton, D.W. (1994). Use of double-replacement gene targeting to replace the murine alpha-lactalbumin gene with its human counterpart in embryonic stem cells and mice. Mol. Cell. Biol. *14*, 1009–1016.

Suchyna, T.M., Nitsche, J.M., Chilton, M., Harris, A.L., Veenstra, R.D., and Nicholson, B.J. (1999). Different ionic selectivities for connexins 26 and 32 produce rectifying gap junction channels. Biophys. J. *77*, 2968–2987.

Suga, Y., Jarnik, M., Attar, P.S., Longley, M.A., Bundman, D., Steven, A.C., Koch, P.J., and Roop, D.R. (2000). Transgenic mice expressing a mutant form of loricrin reveal the molecular basis of the skin diseases, Vohwinkel syndrome and progressive symmetric erythrokeratoderma. J. Cell Biol. *151*, 401–412.

Svitkina, T.M., Shevelev, A.A., Bershadsky, A.D., and Gelfand, V.I. (1984). Cytoskeleton of mouse embryo fibroblasts. Electron microscopy of platinum replicas. Eur. J. Cell Biol. *34*, 64–74.

Theis, M., Mas, C., Döring, B., Krüger, O., Herrera, P., Meda, P., and Willecke, K. (2001). General and conditional replacement of connexin43-coding DNA by a lacZ reporter gene for cell-autonomous analysis of expression. Cell Commun. Adhes. *8*, 383–386.

Thomas, M.A., Zosso, N., Scerri, I., Demaurex, N., Chanson, M., and Staub, O. (2003). A tyrosine-based sorting signal is involved in connexin43 stability and gap junction turnover. J. Cell Sci. *116*, 2213–2222.

Toyofuku, T., Yabuki, M., Otsu, K., Kuzuya, T., Hori, M., and Tada, M. (1998). Direct association of the gap junction protein connexin-43 with ZO-1 in cardiac myocytes. J. Biol. Chem. *273*, 12725–12731.

Turksen, K., and Troy, T.C. (2002). Permeability barrier dysfunction in transgenic mice overexpressing claudin 6. Development *129*, 1775–1784.

van Steensel, M.A., van Geel, M., Nahuys, M., Smitt, J.H., and Steijlen, P.M. (2002). A novel connexin 26 mutation in a patient diagnosed with keratitis-ichthyosis-deafness syndrome. J. Investig. Dermatol. *118*, 724–727.

Willecke, K., Eiberger, J., Degen, J., Eckardt, D., Romualdi, A., Güldenagel, M., Deutsch, U., and Söhl, G. (2002). Structural and functional diversity of connexin genes in the mouse and human genome. Biol. Chem. *383*, 725–737.

Yan, G.X., and Antzelevitch, C. (1999). Cellular basis for the Brugada syndrome and other mechanisms of arrhythmogenesis associated with ST-segment elevation. Circulation *100*, 1660–1666.

Yeager, M., and Gilula, N.B. (1992). Membrane topology and quaternary structure of cardiac gap junction ion channels. J. Mol. Biol. *223*, 929–948.

Zhou, L., Kasperek, E.M., and Nicholson, B.J. (1999). Dissection of the molecular basis of pp60(v-src) induced gating of connexin 43 gap junction channels. J. Cell Biol. *144*, 1033–1045.